A Novel Type of Internal Barium Block of a Maxi-K^+ Channel from Human Vas Deferens Epithelial Cells

Y. Sohma,* A. Harris,# B. E. Argent,* and M. A. Gray*

*Department of Physiological Sciences, University Medical School, Newcastle upon Tyne NE2 4HH, and #Paediatric Molecular Genetics, Institute of Molecular Medicine, Oxford University, John Radcliffe Hospital, Oxford OX3 9DU, England

ABSTRACT We have recently shown that a maxi-K^+ channel from vas deferens epithelial cells contains two Ba^{2+}-binding sites accessible from the external side: a "flickering" site located deep in the channel pore and a "slow" site located close to the extracellular mouth of the channel. Using the patch-clamp technique, we have now studied the effect of internal Ba^{2+} on this channel. Cytoplasmic Ba^{2+} produced a voltage- and concentration-dependent "slow" type of block with a dissociation constant of ~100 μM. However, based on its voltage dependence and sensitivity to K^+ concentration, this block was clearly different from the external "slow" Ba^{2+} block previously described. Kinetic analysis also revealed a novel "fast flickering" block restricted to channel bursts, with an unblocking rate of ~310 s^{-1}, some 10-fold faster than the external "flickering" block. Taken together, these results show that this channel contains multiple Ba^{2+}-binding sites within the conduction pore. We have incorporated this information into a new model of Ba^{2+} block, a novel feature of which is that internal "slow" block results from the binding of at least two Ba^{2+} ions. Our results suggest that current models for Ba^{2+} block of maxi-K^+ channels need to be revised.

INTRODUCTION

Calcium-activated, voltage-dependent maxi-K^+ channels are widely distributed and occur in both excitable and nonexcitable cells. They are involved in regulating a number of important functions, such as cell excitability, vascular tone, electrolyte transport, and volume regulation (McManus, 1991). Recent molecular studies have shown that these channels belong to a superfamily of voltage-gated K^+ channels that includes the archetypal *Shaker* K^+ channel and the erg-related K^+ channels. Members of this superfamily all contain a conserved α-subunit that consists of six putative transmembrane domains (S1–S6) and an H5 segment between S5 and S6 that is suggested to form the channel pore (Pongs, 1992).

Barium ions are known to block a large variety of K^+ channels, including members of this superfamily, and they have been a useful probe for investigating the mechanisms of ion conduction. At the molecular level, recent site-directed mutagenesis studies on *Shaker* K^+ channels (Slesinger et al., 1993; Lopez et al., 1994; Hurst et al., 1996) have identified regions in the S4-S5 loop, the S6 domain, and the pore region, which are involved in barium block. However, similar molecular studies have not yet been performed on maxi-K^+ channels.

Received for publication 28 May 1997 and in final form 30 September 1997.

Address reprint requests to Dr. M. A. Gray, Department of Physiological Sciences, University Medical School, Framlington Place, Newcastle upon Tyne NE2 4HH, England. Tel.: +44-191-222-7592; Fax: +44-191-222-6706; E-mail: m.a.gray@ncl.ac.uk.

Dr. Sohma's present address is Department of Physiology, Osaka Medical College, Takatsuki Osaka 569, Japan.

© 1998 by the Biophysical Society

0006-3495/98/01/199/11 $2.00

At the single-channel level, the effect of Ba^{2+} has been tested on maxi-K^+ channels from both native tissues (Vergara and Latorre, 1983; Benham et al., 1985; Miller, 1987; Brown et al., 1988; Sheppard et al., 1988) and cloned maxi-K^+ channels from *Drosophila* (*dSlo*) (Perez et al., 1994) and human myometrium (*hSlo*) (Diaz et al., 1996). In all of these studies, Ba^{2+} reduced channel activity in a voltage-dependent manner and induced the appearance of long-lived closing (blocking) events lasting for seconds (slow block). Detailed kinetic analysis showed that Ba^{2+} only entered an open channel, where it then bound tightly to a single, well-defined site located within the channel pore, and blocked K^+ permeation. Moreover, based on the effects of K^+ concentration on Ba^{2+} block, Neyton and Miller (1988a,b) proposed that the conduction pathway of the skeletal muscle maxi-K^+ channel contained at least four ion-binding sites: two lock-in K^+ sites located at the internal and external sides of the channel, an external enhancement K^+ site, and a single Ba^{2+}-binding site.

Our recent study (Sohma et al., 1996), which explored the effect of Ba^{2+} on a maxi-K^+ channel obtained from human vas deferens epithelial cells, indicated that a single Ba^{2+}-binding site was not sufficient to explain the type of block we observed. From kinetic analysis we proposed that this maxi-K^+ channel had at least two distinct Ba^{2+}-binding sites accessible from the extracellular side; one was located deep in the channel pore close to the cytoplasmic side of the channel and caused a "flickering" type of block, and the other was located close to the extracellular mouth of the channel and produced a "slow" type of block (Sohma et al., 1996).

Because many of the earlier models of channel block were based on experiments in which Ba^{2+} was applied to the intracellular surface of the channel, we decided to ex-

tend our studies by investigating in detail the properties of internal block of the vas deferens maxi-K^+ channel.

MATERIALS AND METHODS

Human vas deferens cell culture

Primary monolayers of vas deferens cells were grown on collagen-coated glass coverslips from explants of second-trimester human fetal vas deferens as previously described (Harris and Coleman, 1989). Three normal fetuses obtained within 48 h of midtrimester prostaglandin-induced terminations or spontaneous abortions were used in this study. Once established, two main cell types predominate in the cultures; a large angular cell type that does not appear to be tightly packed, even at confluence, and a relatively small "cobblestone" cell type that always appears in tightly packed colonies. Both cell types have been identified as epithelial cells on the basis of morphological, biochemical, and immunocytochemical evidence (Harris and Coleman, 1989). The cultures were passaged onto glass coverslips (passage numbers were between 1 and 6), and 2–4 days later were sent from Oxford to Newcastle upon Tyne. After arrival in Newcastle, they were incubated for 1–7 days in standard growth medium (Harris and Coleman, 1989) minus cholera toxin before electrophysiological studies were performed.

Measurement of single-channel activity

We studied a total of 33 coverslip cultures (between 5 and 18 coverslips from each of the three fetuses). Single-channel recordings were made at 21–23°C using the patch-clamp technique (Hamill et al., 1981). All patches were obtained from the upper surface of small "cobblestone" cells in confluent areas of the monolayers. Full details of the electrophysiological technique used in this study are described elsewhere (Gray et al., 1990). The tissue bath was grounded, and the potential difference across excised, inside-out patches (V_m) was referenced to the extracellular face of the membrane. Junction potentials were measured using a flowing 3 M KCl electrode (Gray et al., 1988), and the appropriate corrections applied to our data.

The Na^+-rich, extracellular-type solution had the following composition (in mM): 138 NaCl, 4.5 KCl, 2 $CaCl_2$, 1 $MgCl_2$, 5 glucose, 10 HEPES at pH 7.4. The 25 K^+/115 Na^+ solution contained 115 NaCl, 25 KCl, 2 $CaCl_2$, 1 $MgCl_2$, 5 glucose, 10 HEPES at pH 7.4. The K^+-rich, intracellular-type solution contained 140 KCl, 2 $CaCl_2$, 1 $MgCl_2$, 5 glucose, 10 HEPES at pH 7.4. When these solutions were used in the pipette, the Ca^{2+} concentration in these solutions was stabilized to 1 μM with a buffer system that contained 2 mM EGTA, glucose was omitted, and they were filtered through a 0.2-μm membrane filter. The free Ca^{2+} and Mg^{2+} concentrations in these solutions were calculated with the EQCAL program (Biosoft). All other chemicals were purchased from commercial sources and were of the highest purity available.

Data analysis

To determine open-state probability (P_0), mean open time (t_o), and mean close time (t_c), current records were digitized at 200–10 kHz with a CED 1401 interface (Cambridge Electric Design) and analyzed with a two-threshold transition algorithm that employed a 50% threshold crossing parameter to detect events. P_0 was calculated as the fraction of total time that channels were open, for a minimum of 60 sec of data. When multichannel patches were used for these determinations, we assumed that the total number of channels present was equal to the maximum number of simultaneous current transitions and that channels open and close independently of one another (Sohma et al., 1994). In our previous paper (Sohma et al., 1994), we reported that in the absence of barium, this maxi-K^+ channel has at least two open and two closed states. The faster open-closed kinetic state has submillisecond durations (t_{o1} = ~0.2 ms, t_{c1} = ~0.2–0.5 ms). The slower kinetic state has millisecond durations (t_{o2} = ~2–5 ms, t_{c2} = ~1–2 ms). Because the very fast time constants were not affected by the blocker (data not shown), we have simplified our analysis by reducing the number of kinetic states to a single open and closed state, by choosing appropriate bin widths.

We were not able to consistently maintain excised, inside-out patches for long enough periods to obtain sufficient "slow" blocking events to construct reliable closed-time histograms. We therefore used P_o data for kinetic analysis of the "slow" block, because here the contribution of the "fast flickering" block to the reduction of P_o by Ba^{2+} was negligible (<1%).

For kinetic analysis of the "fast flickering" block, we usually used inside-out patches containing only one active channel. However, when we used high Ba^{2+} concentrations (5 mM) and/or depolarized voltages (>20 mV), channel activity was very low (P_o < ~0.01), and it was therefore difficult to obtain sufficient "fast flickering" blocking events from a single channel to make reliable closed-time histograms. To overcome this problem, we used multichannel patches, containing two to four channels, to generate sufficient blocking events. During low activity, channels open in short bursts separated by long blocked periods (see Fig. 1 *A*), and under these conditions it was unusual for more than two channel bursts to overlap. However, any events that did overlap were excluded from subsequent analysis. With this mode of analysis, open-time histograms showed a single exponential distribution, whereas closed-time histograms showed two distinct exponential distributions, corresponding to the channels' nat-

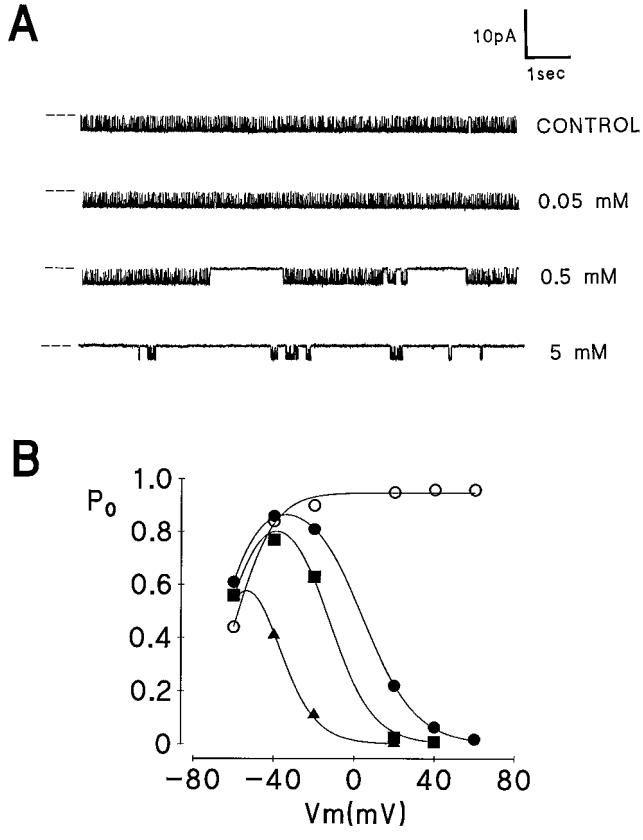

FIGURE 1 Effect of internal Ba^{2+} on maxi-K^+ channel activity. (*A*) Typical single-channel activity recorded from an inside-out patch held at −20 mV in the absence or presence of the indicated Ba^{2+} concentration. Solutions: pipette, K^+-rich; bath, K^+-rich (140:140). Dashed lines indicate the closed state of the channel. Low-pass filtered at 1 kHz. (*B*) Plot of open-state probability (P_o) against V_m. ○, Control; ●, 0.05 mM Ba^{2+}; ■, 0.5 mM Ba^{2+}; ▲, 5.0 mM Ba^{2+}. Lines were fitted by fourth-order polynomial least-squares regression analysis. Current recordings used for analysis were filtered at 5 kHz and digitized at 10 kHz.

ural fast closing events and a novel type of "fast flickering" block (see Fig. 5). These results indicate that all of the channels in a multichannel patch exhibit similar blocking kinetics, validating this approach.

To compare the frequency of Ba^{2+} blocking events at different Ba^{2+} concentrations, we calculated the fractional ratio amplitude of closing events (FRA) as follows:

$$\text{FRA} = (A_{\text{ff}} \cdot t_{\text{ff}})/(A_{\text{c1}} \cdot t_{\text{c1}}) \quad (1)$$

where A_{ff} and t_{ff} and A_{c1} and t_{c1} are the y axis intercept (amplitude), and time constant of the Ba^{2+}-induced fast flickering block and the channels' natural, faster closing events.

Significance of difference between means was determined by using Student's paired or unpaired t-test. Significance of difference between the slopes of population regression lines (i.e., the "fast flickering" blocking rate constant) was determined using analysis of covariance. The level of significance was set at $P \leq 0.05$. All values are expressed as mean ± SEM (number of observations).

RESULTS

Fig. 1 shows the basic characteristics of internal Ba^{2+} block of a maxi-K^+ channel obtained from the apical membrane of a human vas deferens epithelial cell. Fig. 1 *A* shows single-channel current records from an inside-out patch bathed with symmetrical K^+-rich solutions containing 0, 0.05, 0.5, and 5.0 mM Ba^{2+} in the bath, recorded at a holding potential of −20 mV. On this slow time base, it is clear that internal Ba^{2+} blocks the channel and introduces long-lived closed periods lasting many seconds. Fig. 1 *B* summarizes the effect of cytoplasmic Ba^{2+} on the open probability (P_o) of the channel. These data show that barium block is both voltage and concentration dependent, a finding previously described by many investigators (Vergara and Latorre, 1983; Benham et al., 1985; Miller, 1987; Brown et al., 1988; Sheppard et al., 1988).

Although the slow block was the major reason for the decrease in P_o, careful kinetic analysis revealed an additional faster type of channel block during bursts of channel openings. Fig. 2 *A* shows single-channel records displayed on a faster time base for a control channel (Fig. 2 *A*(*a*)) and a channel exposed to 5 mM internal Ba^{2+} (Fig. 2 *A*(*b*)), obtained at −20 mV. Inspection of these records shows that Ba^{2+} caused the channel to undergo rapid blocking events lasting for milliseconds. Fig. 2, *B* and *C*, shows the open- and closed-time histograms for these data, obtained from a single channel that maintained stable activity for more than an hour. Without Ba^{2+}, the open- and closed-time histograms had an exponential distribution. Note that the very rapid (submillisecond) opening events that we have previously reported for this channel (Sohma et al., 1994) were effectively removed by choosing appropriate bin widths for the sake of simplifying the analysis (Materials and Methods), and that the control closed-time histogram usually showed an additional, smaller, and slower distribution under this condition (see Fig. 5). In the presence of Ba^{2+} the mean open time (t_{oBa}: 2.19 ± 0.13 ms, $n = 5$) was significantly smaller than in the absence of Ba^{2+} (t_o: 3.62 ± 0.63 ms, $n = 5$). For the closed-time histogram, two additional, slower distributions were apparent, with time constants on the order of 3.4 ms and 3.0 s (see Fig. 2, *C*(*a*) and *C*(*b*)). For the faster kinetics (Fig. 2 *C*(*a*)), the data were best fitted by the sum of two exponential functions. The faster component had a mean closed time in the presence of Ba^{2+} (t_{cBa}) of 0.40 ± 0.05 ms ($n = 5$), which was not significantly different from that in the control (t_{c1} = 0.49 ± 0.09 ms, $n = 5$), and

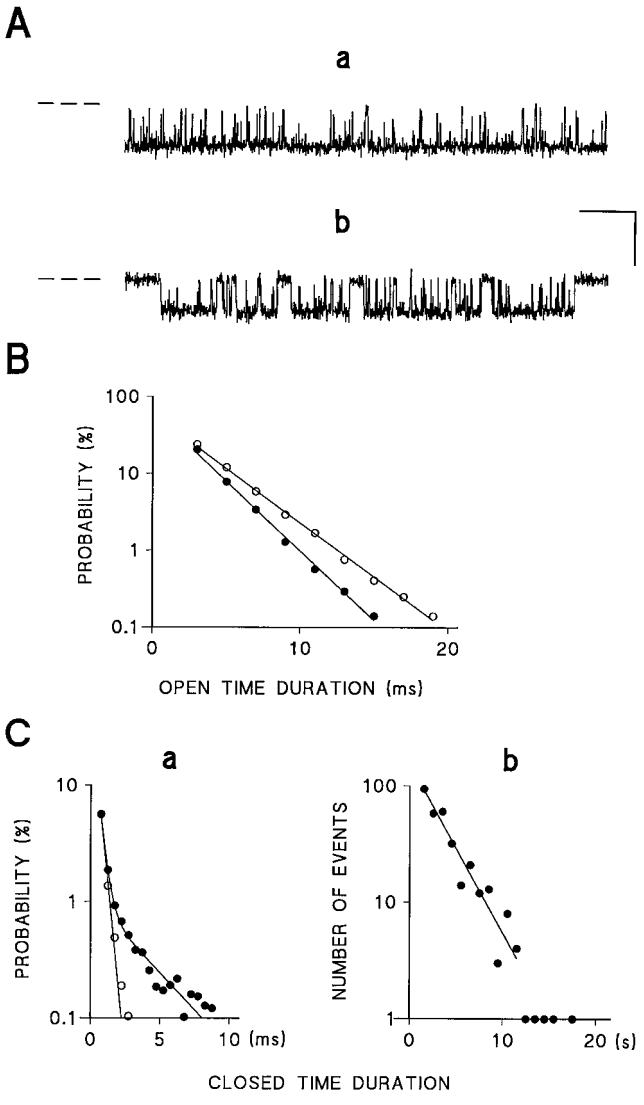

FIGURE 2 Internal Ba^{2+} produces two types of channel block. (*A*) Single-channel current records displayed on a faster time-base (*a*) without and (*b*) with 5 mM internal Ba^{2+}. Same conditions as in Fig. 1. Scale indicates 50 ms (*horizontal*) and 5 pA (*vertical*), respectively. Low-pass filtered at 2 kHz. (*B* and *C*) Semilog plots of (*B*) open- and (*C*) closed-time histograms for control (○) and a channel exposed to 5 mM internal Ba^{2+} (●). Open-time distributions were fitted by a single exponential with time constants of 3.1 (○) and 2.4 ms (●), respectively. The bin width of the histogram is 2 ms. The closed-time distribution for the control was fitted by a single exponential with a time constant of 0.35 ms. The closed-time distribution with Ba^{2+} was fitted by three exponentials with time constants of 0.37 ms, 3.4 ms, and 3.0 s. The bin widths are (*a*) 0.5 ms and (*b*) 1 s. The current recordings used for analysis in *B* and *C*(*a*) were filtered at 5 kHz and digitized at 10 kHz. The current recording used for analysis in *C*(*b*) was recorded for 1690 s, filtered at 100 Hz, and digitized at 200 Hz. P_0 = 0.93 in control and 0.12 with Ba^{2+}.

represents the normal fast gating of the channel. The novel component seen in the presence of Ba^{2+} had a mean closed time of 2.89 ± 0.57 ms ($n = 5$). Overall, these data show that application of cytoplasmic Ba^{2+} caused a classical "slow" block as well as a novel "fast flickering" block lasting for milliseconds. That Ba^{2+} decreased t_o but did not significantly change t_{c1} suggests that both forms of internal block occur according to an open channel blocking scheme.

The "fast flickering" blocking events described here are considerably faster than we previously reported for external Ba^{2+} block (Sohma et al., 1996) and resemble the channels' natural closing state. Moreover, this block is only seen during bursts of channel openings. With higher Ba^{2+} concentrations, in which the "fast flickering" block should occur more frequently, the burst length becomes shorter (Fig. 1 *A*), and the frequency of blocking events actually observed is decreased. This is one reason why it was initially hard to identify the "fast flickering" block. In terms of reducing P_o, the "slow" block was predominant and the contribution of the faster block to the reduction of P_o is estimated to be ~1% of the total blocked time.

Characteristics of internal slow block

The characteristics of the "slow" block were studied by using P_o data because of the difficulty in obtaining sufficient blocking events for lifetime distributions. In the following analysis, we have assumed that 1) block occurred according to an open channel blocking scheme, and 2) in the absence of blocker, the natural gating of the channel consisted of a single closed and open state (Fig. 2). In this way, internal "slow" Ba^{2+} block can be described by the kinetic model below:

$$\underset{\text{closed}}{C} \underset{\alpha}{\overset{\beta}{\leftrightarrow}} \underset{\text{open}}{O} + Ba^{2+} \underset{k_{s-1}}{\overset{k_{s1}[Ba^{2+}]}{\longleftrightarrow}} \underset{\text{open blocked}}{OBa^{2+}}$$

(Scheme 1)

where k_{s1} and k_{s-1} are the blocking and unblocking rate constants of the slow Ba^{2+} block, respectively.

By using Scheme 1, the kinetics of Ba^{2+} block can be obtained from the relationship (Benham et al., 1985)

$$K_d(V_m) = [Ba^{2+}] \cdot P_o\text{block} \cdot P_o\text{control}/(P_o\text{control-}P_o\text{block}) \quad (2)$$

where $K_d(V_m)$ is the voltage-dependent dissociation constant, and $P_o$block and $P_o$control are the open probabilities in the presence and absence of Ba^{2+}, respectively. Because the contribution of the "fast flickering" block to the reduction of P_o is negligible (<1%), $K_d(V_m)$ represents the kinetics of "slow" block.

In our previous report (Sohma et al., 1996), we found that external Ba^{2+} block showed a strong dependence on K^+ concentration. Fig. 3 summarizes the effect of changing both cytoplasmic and extracellular K^+ concentration on internal "slow" Ba^{2+} block. Fig. 3, *A–D*, shows data at three different Ba^{2+} concentrations measured over a range of voltages. These semilog plots of $K_d/[Ba^{2+}]$ against voltage are essentially linear under all of the conditions tested. Therefore, $K_d(V_m)$ can be described as

$$K_d(V_m) = K_d(0) \cdot \exp(-z\delta FV_m/RT) \quad (3)$$

where $K_d(0)$ is a dissociation constant at 0 mV; $z\delta$ is an apparent effective valence of the blocking reaction; and R, T, and F have their usual meanings (Woodhull, 1973). Fig. 3, *E* and *F*, shows that both $K_d(0)$ and $z\delta$ were essentially independent of Ba^{2+} concentration, but were affected by K^+ concentration. We therefore pooled all of the K_d data at the various Ba^{2+} concentrations. Overall, these data show that at the same voltage and Ba^{2+} concentration, changes in the concentration of K^+ in both the intracellular and extracellular solutions affect the amount of block, but not the "slow" blocking kinetics. In addition, changes in extracellular K^+ had more pronounced effects on Ba^{2+} block than changes in cytoplasmic K^+ concentration (compare Fig. 3 *A* with Fig. 3 *D*).

Fig. 4 *A* shows that K_d varied exponentially with voltage and altered as extracellular K^+ concentration changed. Fig. 4, *B* and *C*, illustrates the effect of extracellular K^+ concentration, $[K^+]_{ex}$, on $K_d(0)$ and $z\delta$, respectively. With a fixed cytoplasmic K^+ concentration of 140 mM, increasing $[K^+]_{ex}$ from 4.5 to 140 mM increased $K_d(0)$ from $1.1 \times 10^{-6} \pm 7.2 \times 10^{-8}$ ($n = 5$) to $1.0 \times 10^{-4} \pm 1.2 \times 10^{-5}$ ($n = 8$); $z\delta$ also increased from 1.08 ± 0.06 ($n = 5$) to 2.34 ± 0.09 ($n = 8$). Both log $K_d(0)$ and $z\delta$ saturated with increasing $[K^+]_{ex}$ with saturation constants, K_{DK}, of 46.0 mM and 51.6 mM, respectively. When extracellular K^+ was kept constant at 140 mM, decreasing the cytoplasmic K^+ concentration from 140 to 4.5 mM increased $K_d(0)$ significantly from $1.0 \times 10^{-4} \pm 1.2 \times 10^{-5}$ ($n = 8$) to $3.0 \times 10^{-4} \pm 2.2 \times 10^{-5}$ (Fig. 4 *B*, *open circles*, $n = 10$ $p < 0.01$) but did not change $z\delta$ significantly (Fig. 4 *C*, *open circle* overlaps *closed circle* at 145 mM $[K^+]_{ex}$).

Neyton and Miller (1988a,b) suggested that bound Ba^{2+} could dissociate from its binding site to either the internal or external side of the skeletal muscle maxi-K^+ channel, depending on conditions. This process can be described by the scheme below:

$$\underset{\text{(Cyt)}}{\underset{\text{open}}{O} + Ba^{2+}} \underset{k_{s-1}}{\overset{k_{s1}}{\longleftrightarrow}} \underset{\text{blocked}}{OBa^{2+}} \overset{k_{s2}}{\longrightarrow} \underset{\text{(Ext)}}{\underset{\text{open}}{O} + Ba^{2+}}$$

(Scheme 2)

According to Scheme 2,

$$\begin{aligned} K_d(V_m) &= (k_{s-1} + k_{s2})/k_{s1} \\ &= K_{d1} + K_{d2} \\ &= K_{d1}(0) \cdot \exp(-z\delta_1 FV_m/RT) \\ &\quad + K_{d2}(0) \cdot \exp(-z\delta_2 FV_m/RT) \end{aligned} \quad (4)$$

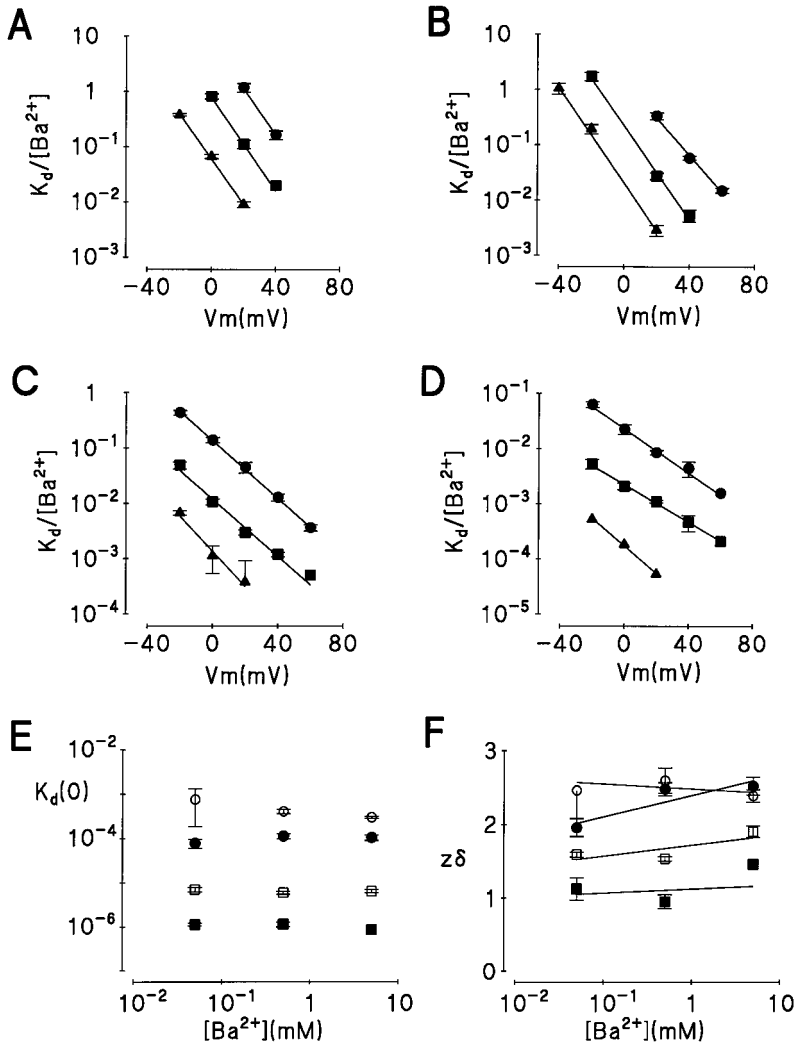

FIGURE 3 Summary of the effect of voltage and K^+ concentration on the kinetics of slow Ba^{2+} block. (*A–D*) Semilog plots of the dissociation constant (K_d/Ba^{2+}) against voltage. K^+ concentrations (in mM; pipette: bath): (*A*) 140:4.5 (n = 10), (*B*) 140:140 (n = 8), (*C*) 25:140 (n = 5), (*D*) 4.5:140 (n = 5). Ba^{2+} concentrations: ●, 0.05 mM; ■, 0.5 mM; ▲, 5.0 mM. (*E*) Log-log plot of the dissociation constant at 0 mV, $K_d(0)$, against Ba^{2+} concentration. (*F*) Semilog plot of effective valence ($z\delta$) against Ba^{2+} concentration. K^+ concentrations (in mM; pipette:bath): ○, 140:4.5 (n = 10); ●, 140:140 (n = 8); □, 25:140 (n = 5); ●, 4.5:140 (n = 5). $K_d(0)$ and $z\delta$ were calculated using Eq. 3. Lines were fitted by first-order least-squares regression analysis.

where $K_{d1}(0)$ and $K_{d2}(0)$ are "directional" zero-voltage dissociation/association constants for Ba^{2+} dissociating to the cytoplasmic and extracellular sides, respectively, and $z\delta_1$ and $z\delta_2$ are the respective effective valences. We applied Scheme 2 to the K_d data shown in Fig. 4 *A* by using Eq. 4. Fig. 4 *D* shows that these data were well described by Scheme 2 and that overall, Eq. 4 gave a better fit to the data points than an exponential function. The advantage of this scheme is that it allows us to fit the K_d data with a common set of constant effective valences, $z\delta_1$ and $z\delta_2$, over the four different $[K^+]$ conditions. Table 1 shows the values of $K_{d1}(0)$ and $K_{d2}(0)$ obtained by fitting Eq. 4 to the K_d data in Fig. 4 *D*. With $[K^+]_{cyt}$ = 140 mM, increasing $[K^+]_{ex}$ increased both $K_{d1}(0)$ and $K_{d2}(0)$. The value of $K_{d1}(0)/K_{d2}(0)$ also increased from 0.11 to 12.0 when $[K^+]_{ex}$ increased from 4.5 mM to 140 mM. This suggests that Ba^{2+} predominately dissociates to the extracellular side of the channel when $[K^+]_{ex}$ = 4.5 mM, and conversely, it dissociates to the cytoplasmic side when $[K^+]_{ex}$ = 140 mM. With $[K^+]_{ex}$ = 25 mM, $K_{d1}(0)/K_{d2}(0)$ was equal to 1.0, implying that under this condition Ba^{2+} dissociated equally to the cytoplasmic and extracellular sides.

Characteristics of the fast flickering block

Fig. 5 shows the effect of 0.5 mM and 5.0 mM internal Ba^2 on the open- and closed-time histograms for channels bathed with asymmetrical K^+-rich solutions (140 pip:4.5 bath) and studied at voltages between ±20 mV. Note that for these data we have ignored the much longer-lived blocking events. In the absence of blocker, the open-time histograms showed a exponential distribution with time constants, t_o, on the order of 10 ms (see Table 2). The effect of Ba^{2+} was to decrease open times (t_{oBa}), and this was dependent on the Ba^{2+} concentration (Fig. 5 *C* and Table 2).

The control closed-time histograms were best fit by the sum of two exponential functions at −20 and 0 mV, and by a single exponential at 20 mV (Fig. 5, *open circles*). The faster time constant (t_{c1}) was essentially voltage-independent and some three- to fourfold faster than the slower time constant (t_{c2}) (see Table 2). In the presence of internal Ba^{2+} a new, slower distribution appeared on the closed-time histogram (t_{cfm}) that was approximately threefold slower than t_{c2}. It should be noted that even at −20 mV and 0 mV, at which the control closed-time histogram showed a double

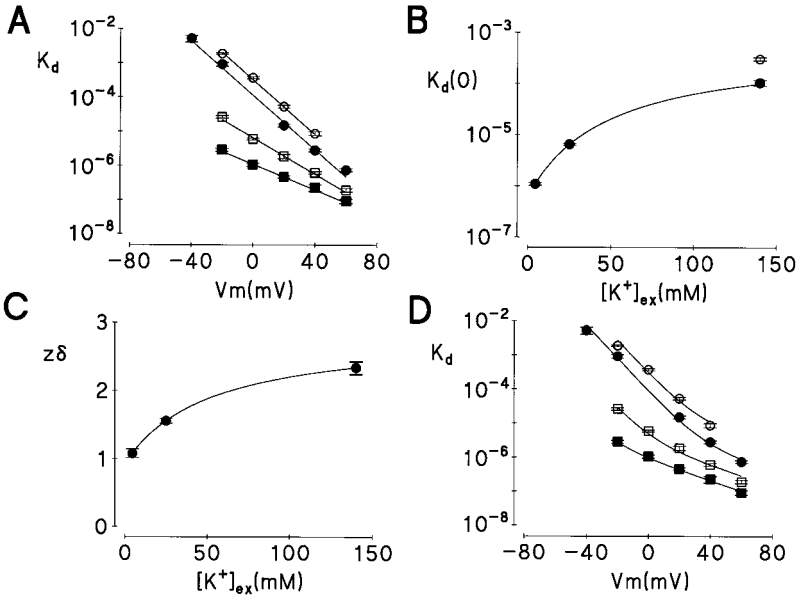

FIGURE 4 Characteristics of slow Ba^{2+} block. (*A*) Voltage dependence of K_d. K^+ concentrations (in mM; pipette:bath): ○, 140:4.5 ($n = 10$); ●, 140:140 ($n = 8$); □, 25:140 ($n = 5$); ■, 4.5:140 ($n = 5$). Data were calculated from Fig. 3. The lines were fitted by first-order least-squares regression analysis. (*B*, *C*) Effect of extracellular K^+ activity on (*B*) $K_d(0)$ and (*C*) $z\delta$. Bath K^+ concentrations: ○, 4.5; ●, 140 mM. Data are from Fig. 3. The lines were fitted using the following equations: (*B*) $\log K_d(0) = a + (b - a)/(1 + K_{DK}/[K^+]_{ex})$ with $K_{DK} = 46.0$ mM ($a = 5.9 \times 10^{-7}$, $b = 5.3 \times 10^{-4}$); (*C*) $z\delta = a + (b - a)/(1 + K_{DK}/[K^+]_{ex})$ with $K_{DK} = 51.6$ mM ($a = 0.92$, $b = 2.86$). (*D*) Experimental and calculated voltage dependence of K_d for internal Ba^{2+} block. Experimental data from Fig. 4 *A*. Solid lines were fitted to Eq. 4. Fitted parameters are shown in Table 1.

exponential distribution, the closed-time histogram with Ba^{2+} was still best described by the sum of two exponential functions (Fig. 5, *A* and *B*). Occasionally, at −20 mV and with 5 mM Ba^{2+}, the closed-time histogram needed three exponentials to fit the data (data not shown). The very fast closed time constants (t_{c1Ba}) were not significantly altered by the presence of 5 mM Ba^{2+} (Table 2).

Fig. 6, *A* and *B*, summarizes the effect of Ba^{2+} on mean open and mean closed times. It is clear that Ba^{2+} reduced mean open times voltage dependently, and this was also dependent on blocker concentration (Fig. 6 *A*). Note that the voltage dependences of t_o and t_{oBa} are quite different, which excludes the possibility that block is due simply to a shift in the voltage-gating curve of the channel toward more depolarized potentials (caused, e.g., by an electrostatic effect of Ba^{2+} or by channel run-down). The frequency of the blocking events was also dependent on Ba^{2+} concentration (at 20 mV with 5 mM Ba^{2+}, FRA = 0.16 ± 0.03, $n = 5$; with 0.5 mM Ba^{2+}, FRA = 0.035 ± 0.008, $n = 4$, $p = 0.01$). The t_{cfm} was largely voltage independent with asymmetrical K^+-rich solutions (Fig. 6 *B*), but was dependent on Ba^{2+} concentration. At $V_m = 20$ mV, $t_{cfm} = 3.39 \pm 0.24$ ms ($n = 5$) with 5 mM Ba^{2+}. This is significantly slower than 2.16 ± 0.24 ms with 0.5 mM Ba^{2+} ($n = 4$, $p = 0.009$). This suggests that there might be a lock-in site with affinity for Ba^{2+} located at the cytoplasmic side of the "fast flickering" site. If this were the case, Ba^{2+} binding to this lock-in site would prevent bound Ba^{2+} from dissociating to the cytoplasmic side of the channel. A similar lock-in effect by Ba^{2+} was reported by Neyton and Pelleschi (1991) for the rat skeletal muscle maxi-K^+ channel.

TABLE 1 Values of $K_{d1}(0)$ and $K_{d2}(0)$ for slow barium block

Solution $[K^+]_{ex}$:$[K^+]_{cyt}$ (mM)	$K_{d1}(0)$ (M)	$K_{d2}(0)$ (M)	$K_{d1}(0)/K_{d2}(0)$
4.5:140	1.0×10^{-7}	8.9×10^{-7}	0.11
25:140	2.5×10^{-6}	2.5×10^{-6}	1.0
140:140	8.4×10^{-5}	6.9×10^{-6}	12.0
140:4.5	2.8×10^{-4}	3.3×10^{-5}	8.4

Values were obtained by fitting Eq. 4 to the data in Fig. 4 *D*, where $z\delta_1 = 2.86$ and $z\delta_2 = 0.92$.

The data presented in Fig. 2 suggested that the "fast flickering" Ba^{2+} block occurred according to an open channel blocking scheme. It is therefore possible to use a simplified kinetic model for the analysis of this type of block as follows:

closed2 closed1 open open blocked

$$\left(C2 \underset{\alpha_2}{\overset{\beta_2}{\leftrightarrow}}\right) \quad C1 \quad \underset{\alpha_1}{\overset{\beta_1}{\leftrightarrow}} O + Ba^{2+} \underset{k_{ff-1}}{\overset{k_{ff1}\cdot[Ba^{2+}]}{\leftrightarrow}} \quad OBa^{2+}$$

(Scheme 3)

where the closed states 1 and 2 correspond to the channels' natural faster closed time distributions (see Materials and Methods). For the sake of simplicity, the channels' natural open-closed kinetic scheme has been reduced to one open and two closed states, although the natural slower closed state (closed2, in parentheses) is difficult to resolve at depolarized potentials (>20 mV). Note that in this scheme, increasing $[Ba^{2+}]$ increases the probability of the channel existing in the blocked state, OBa, and decreases the probability of the channel existing in the other states, including the closed2 state. Moreover, t_{c2} (~0.5–1.5 ms) is relatively close to t_{cfm} (~2–3 ms), so that the natural slower distribution could be buried in the Ba^{2+}-induced distribution.

In the presence of Ba^{2+}, the mean open time (t_{oBa}) is described by the backward rate constant, α_1, and the "fast flickering" blocking rate constant, k_{ff1}, so that

$$t_{oBa} = 1/(\alpha_1 + k_{ff1} \cdot [Ba^{2+}]) \qquad (5)$$

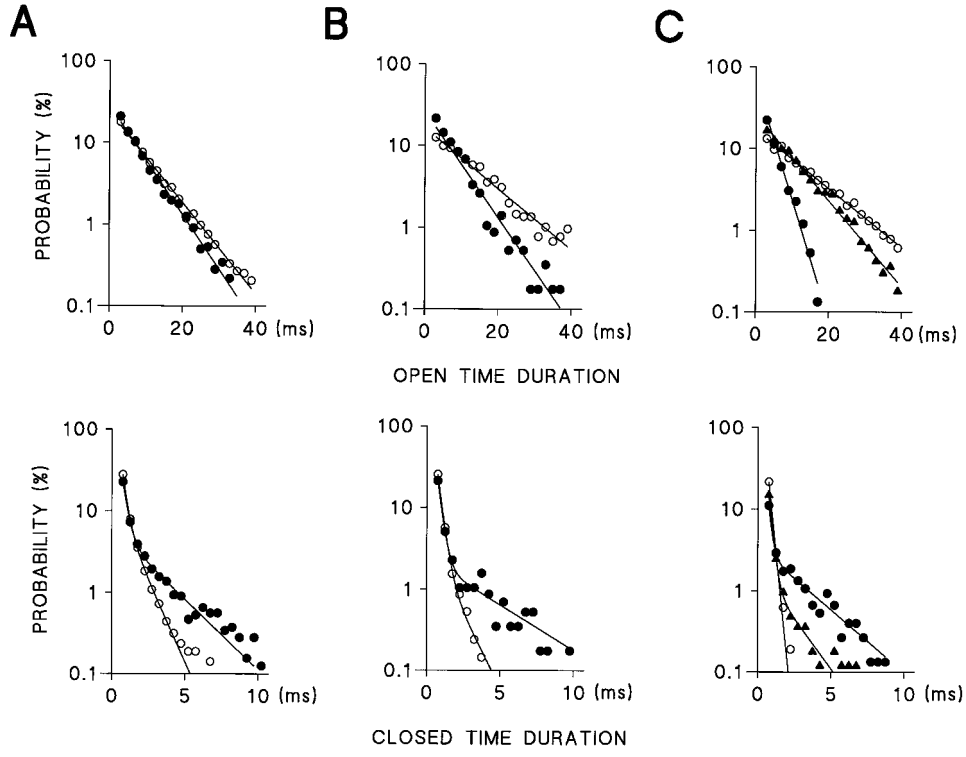

FIGURE 5 Kinetics of the fast flickering block. (*A–C*) Semilog plots of open- and closed-time histograms obtained at (*A*) −20 mV, (*B*) 0 mV, and (*C*) 20 mV. ○, control; ▲, channel exposed to 0.5 mM Ba^{2+}; ●, channel exposed to 5.0 mM internal Ba^{2+}. All data were obtained from a patch containing a single channel, except for *C*, where data in the presence of 5.0 mM Ba^{2+} were obtained from a patch containing four channels. Open-time distributions were fitted by a single exponential. For data at −20 mV (*A*) time constants were 7.8 ms (○), 6.5 ms (●). At 0 mV (*B*) time constants were 11.7 ms (○), 6.7 ms (●). At 20 mV (*C*) time constants were 12.1 ms (○), 8.3 ms (▲), 3.0 ms (●). Closed-time distributions were fitted by a single or double exponential. For data at −20 mV (*A*), time constants were 0.27 and 1.1 ms (○), and 0.31 and 2.5 ms (●). At 0 mV (*B*), time constants were 0.29 and 1.2 ms (○), and 0.29 and 3.9 ms (●). At 20 mV (*C*), time constants were 0.25 ms (○), 0.23 and 1.8 ms (▲), and 0.20 and 2.8 ms (●). Bin widths were 2 ms for open-time distributions and 0.5 ms for closed-time distributions. Note that the current recordings used for analysis were filtered at 2 kHz and digitized at 5 kHz. Solutions: pipette, K^+-rich; bath, Na^+-rich (140:4.5).

The new Ba^{2+}-induced closed-time distribution (see Figs. 2 and 5), t_{cfm}, is described by the "fast flickering" unblocking rate constant, k_{ff-1}, so that

$$t_{cfm} = 1/k_{ff-1} \quad (6)$$

Therefore, k_{ff1} and k_{ff-1} are described by

$$k_{ff1} = (1/t_{oBa} - 1/t_o)/[Ba^{2+}] \quad (7)$$

and

$$k_{ff-1} = 1/t_{cfm} \quad (8)$$

Because k_{ff1} was not significantly dependent on barium concentration between 0.5 and 5 mM (by analysis of covariance, $p = 0.79$), this suggests that the on rate of the fast flickering block ($k_{ff1} \cdot [Ba^{2+}]$) changes proportionally with changes in Ba^{2+} concentration, as would be predicted for a bimolecular process. On the other hand, k_{ff-1} was significantly dependent on barium concentration. Therefore we have used the value of k_{ff-1} obtained with 5 mM Ba^{2+} for further analysis.

Fig. 6 *C* shows the voltage dependence of k_{ff1} and k_{ff-1}. With a K^+-rich pipette and a Na^+-rich bath solution, the

TABLE 2 Effect of internal barium on mean open and mean closed times

	Open-time distribution		Closed-time distribution			
V_m (mV)	t_0 (ms)	t_{0Ba} (ms)	t_{c1} (ms)	t_{c2} (ms)	t_{c1Ba} (ms)	t_{cfm} (ms)
+20	13.3 ± 1.2 (5)	3.76 ± 0.41 (5)	0.26 ± 0.02 (5)	—	0.24 ± 0.04 (5)	3.39 ± 0.24 (5)
0	11.1 ± 0.4 (4)	5.67 ± 0.62 (7)	0.26 ± 0.04 (4)	0.69 ± 0.05 (4)	0.30 ± 0.03 (7)	3.45 ± 0.31 (7)
−20	7.79 ± 0.52 (5)	6.10 ± 0.65 (7)	0.30 ± 0.04 (5)	1.16 ± 0.10 (5)	0.36 ± 0.03 (7)	3.01 ± 0.40 (7)

Values are means ± SE, with the number of observations in parentheses. Values were obtained from lifetime distributions described in Fig. 5. $[Ba^{2+}]$ = 5 mM, $[K^+]_{pipette}$:$[K^+]_{bath}$ = 140:4.5 mM.

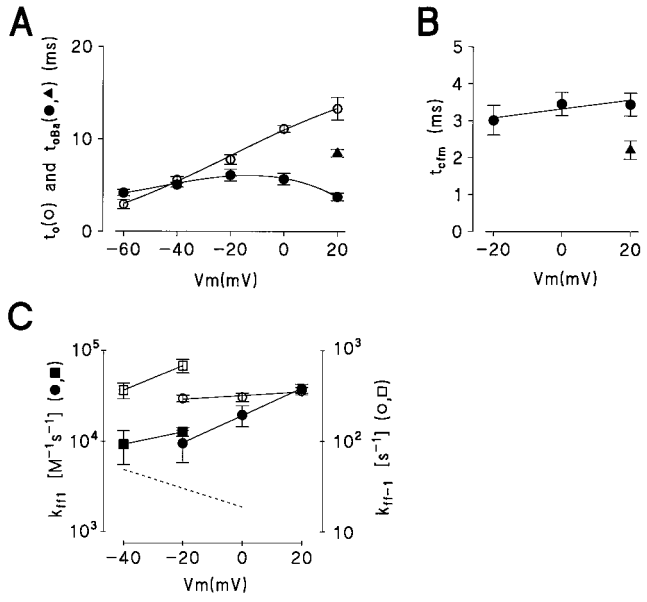

FIGURE 6 Voltage dependence of the fast flickering block. (*A*) Mean open time for control (t_o) (○), 0.5 mM Ba^{2+} (▲), and 5 mM Ba^{2+} (t_{oBa}) (●). (*B*) Mean blocked time (t_{cfm}) induced by 0.5 mM Ba^{2+} (▲) and 5 mM Ba^{2+} (●) at different membrane potentials. The solid lines were fitted by first- or third-order polynomial least-squares regression analysis. Data were obtained from seven single-channel patches and nine multichannel patches, by the analysis described in Materials and Methods. Solutions: pipette, K^+-rich; bath, Na^+-rich (140:4.5). (*C*) Voltage dependence of the blocking rate (k_{ff1}) (●, ■) and the unblocking rate (k_{ff-1}) (○, □). Solutions: ○, ●, pipette, K^+-rich; bath, Na^+-rich (140:4.5). □, ■, pipette, K^+-rich; bath, K^+-rich (140:140). k_{ff1} and k_{ff-1} were calculated from Eqs. 7 and 8, respectively. Linear regression analysis was used for calculating k_{ff1} from unpaired data. The solid lines were fitted by first-order polynomial least-squares regression analysis. For comparison, the dashed line shows the corresponding unblocking rate for the "flickering" block induced by external 5.0 mM Ba^{2+}, with asymmetrical K^+-rich solutions (pipette 140: bath 4.5) (taken from Sohma et al., 1996).

blocking rate constant, k_{ff1}, was voltage dependent (*closed circles*), but the unblocking rate constant, k_{ff-1}, was largely voltage independent (*open circles*) and more than 10-fold faster than the extracellular "flickering" block (20–30 s^{-1}, *dashed line* in Fig. 6 *C*) under the same condition (Sohma et al., 1996). This suggests that the vas deferens maxi-K^+ channel has a low-affinity Ba^{2+} binding site in the channel pore, which is distinct from the "flickering" binding site. Increasing cytoplasmic [K^+] from 4.5 mM to 140 mM (*squares*) increased $k_{ff-1}(0)$ approximately fourfold and changed k_{ff-1} from voltage independent to voltage dependent with positive polarity. This suggests that K^+ entering the channel from the cytoplasmic side "knocks off" Ba^{2+} from the "fast flickering" site, mainly to the extracellular side of the channel under a symmetrical 140 mM K^+ condition. That k_{ff1} was voltage dependent and displayed positive polarity under both symmetrical and asymmetrical K^+-rich conditions indicates that in Scheme 3 Ba^{2+} entering the pore from the internal side binds to the "fast flickering" site.

DISCUSSION

Our results presented here indicate that internal barium causes a complicated type of channel block that is consistent with multiple barium-binding sites within the conduction pathway. Internal Ba^{2+} produced a voltage-dependent "slow" block, with properties similar to those reported by other groups. A much faster type of block (fast flickering block), which has not been described before, has also been identified, and it uses a binding site different from the one underlying "flickering" block (Sohma et al., 1996). Overall, these new data indicate that the vas deferens maxi-K^+ channel has at least two distinct Ba^{2+}-binding sites accessible from the cytoplasmic side of the channel in addition to the two binding sites we have already identified (Sohma et al., 1996).

Characteristics of internal slow barium block

The "slow" Ba^{2+} block showed most of the characteristics previously reported for both native maxi-K^+ channels (Vergara and Miller, 1983; Benham et al., 1985; Miller et al., 1987; Brown et al., 1988; Sheppard et al., 1988) and for cloned maxi-K^+ channels (Perez et al., 1994; Diaz et al., 1996). Block was concentration dependent and followed a single-site inhibition scheme. The K_d was exponentially voltage dependent and was strongly affected by the K^+ concentration in the bathing solutions. The values of $K_d(0)$ (100 μM with symmetrical 140 mM K^+; 1.1 μM with cytoplasmic 4.5 mM and extracellular 140 mM K^+) are in the same range reported for both native and cloned maxi-K^+ channels. The $z\delta$ value (2.3, with symmetrical 140 mM K^+) is also similar to the previous reports.

It has been suggested that relief of internally applied channel blockers by external K^+ could arise from multiple ion occupancy and repulsive interactions between ions in the channel pore (Armstrong, 1975; Yellen, 1984; Hille and Schwarz, 1978). Neyton and Miller (1988b) reported that high external K^+ concentrations (100–1000 mM) increased the dissociation rate of Ba^{2+} applied from the internal side of the channel ("enhancement" effect) in the skeletal muscle maxi-K^+ channel. We have shown here that increasing extracellular K^+ (at constant 140 mM cytoplasmic K^+) also relieved internal Ba^{2+} block and resulted in increases in both $K_d(0)$ and $z\delta$ (Fig. 4, *B* and *C*), which was very similar to the "enhancement" effect reported by Neyton and Miller (1988b). This suggests that the relief might also occur according to a multiion occupancy mechanism and involve a repulsive interaction between Ba^{2+} and K^+.

With a constant extracellular K^+ concentration of 140 mM, decreasing the cytoplasmic K^+ concentration, $[K^+]_{cyt}$, also resulted in an increase in $K_d(0)$. This effect can be partially explained by the internal "lock-in" effect; that is, K^+ binding to a site located at the cytoplasmic side of the blocker binding site reduces the rate of dissociation of Ba^{2+} to the cytoplasmic side (Neyton and Miller, 1988b). In contrast to $K_d(0)$, $z\delta$ was not significantly affected by de-

creasing $[K^+]_{cyt}$ from 140 to 4.5 mM. The simplest interpretation of this result is that with high extracellular K^+, Ba^{2+} mainly dissociates to the cytoplasmic side of the channel at both high and low cytoplasmic K^+ concentrations. This is supported by the analysis using Scheme 1 (Table 1).

Are internal and external slow barium-binding sites the same?

One of the key questions to answer from this present work is whether the internal and external "slow" Ba^{2+}-binding sites are the same. We have shown here that when the channel was bathed with a high extracellular K^+-rich solution, 1) application of internal Ba^{2+} produced a "slow" block, whereas under this condition external Ba^{2+} was previously shown to be ineffective (Sohma et al., 1996), and 2) Ba^{2+} entering the channel from the internal side mainly dissociated back to the same side, which indicates that Ba^{2+} is not able to reach the external "slow" site (see Fig. 4 *D* and Table 1). These two findings make it unlikely that the internal and external "slow" Ba^{2+} sites are the same.

Characteristics of the novel fast flickering barium block

The large difference between the unblocking rates of the "fast flickering" block (k_{ff-1}) and the external "flickering" block (k_{f-1}) we have previously described (Sohma et al., 1996), when measured under the same conditions, suggests that this maxi-K^+ channel has two distinct binding sites responsible for fast channel block. However, the low-affinity Ba^{2+} site identified here did show a "knock-off" effect (Armstrong, 1975) by cytoplasmic K^+ (Fig. 6 *C*), a property also displayed by the "flickering" binding site (Sohma et al., 1996). In addition, we have also described a "lock-in" effect by Ba^{2+} (Neyton and Pelleschi, 1991) on the fast flickering block.

Relationship between "fast flickering" and "slow" block

An important question to consider is whether the "fast flickering" and "slow" sites interact. If we first assume that the two sites do not interact and are located sequentially from the extracellular to cytoplasmic side within a single-file channel pore (Fig. 7 *A*), internal Ba^{2+} should only cause "slow" block. For a scheme in which the sites are located in the opposite orientation (Fig. 7 *B*), as recently described by Hurst et al. (1995, 1996) for fast and slow external Ba^{2+} block of wild-type and mutant *Shaker* K^+ channels, "fast flickering" block should be caused by Ba^{2+} binding to this site and then dissociating back to the cytoplasmic side of the channel. However, Fig. 6 *C* shows that k_{ff-1} decreased with hyperpolarization with symmetrical K^+-rich solutions, which suggests that Ba^{2+} mainly dissociates to the extracellular side. This result is inconsistent with Ba^{2+} binding to the fast site and then dissociating to the cytoplasmic side. In addition, even if Ba^{2+} mainly dissociated to the extracellular side of the channel, "slow" block should have occurred more frequently than the "fast flickering" block in this model, which it clearly did not. Therefore the second two-site model is also inadequate for explaining our experimental data.

A four-state cyclic equilibrium model for barium block

We can summarize the present results and those we have previously reported (Sohma et al., 1996) as follows:

1. External Ba^{2+} produces a "flickering" as well as a voltage-independent "slow" type of channel block.
2. Internal Ba^{2+} produces a "fast flickering" as well as a voltage-dependent "slow" type of channel block.
3. The "flickering" and "fast flickering" block are kinetically distinct and involve separate binding sites.
4. The internal "slow" blocking site is different from the external "slow" blocking site.
5. Both fast types of block as well as the internal "slow" block were observed under conditions in which the blocking ion, during a cycle of binding and unbinding, actually passed through the channel pore.

As described in the previous section, the last finding cannot adequately be explained by a "two independent site" model (Fig. 7, *A* and *B*). We have incorporated this information into a novel blocking model consisting of a four-state cyclic equilibrium of Ba^{2+} binding to an open channel (Fig. 7 *C*). The novel feature of this model is that it includes two single-occupancy Ba^{2+} sites, "fast 1" and "fast 2," connected to a double-occupancy state. The voltage-dependent "slow" form of block (caused by internal Ba^{2+}) is only observed when both sites are occupied, because the Ba^{2+} dissociation rate is decreased under double occupancy. With a single-file channel pore, this new model can explain the experimentally observed characteristics of Ba^{2+} block (1–5), excluding the external "slow" block.

If we now consider the case where Ba^{2+}, entering the channel from either the internal or external solution, dissociates to the *external* side (e.g., under symmetrical K^+-rich conditions), and assuming that $k_{-1} < k_{-2}$ and that $k_{-2} \gg k_{-3}$ (because of the "lock-in" effect of K^+), external Ba^{2+} will first bind to the "fast 2" site and then dissociate back to the external side of the channel, producing "flickering" block (note that under these conditions, the external "slow" site is occupied by K^+ and Ba^{2+} is unable to bind). With internal Ba^{2+} this will first bind to the "fast 1" site and then move to the "fast 2" site and finally dissociate to the extracellular side of the channel, producing the "fast flickering" block. In both cases the unblocking rate should be mainly limited by k_{-1}. This is supported by the fact that the unblocking rates for internal "fast flickering" and external "flickering" are similar under symmetrical K^+ conditions

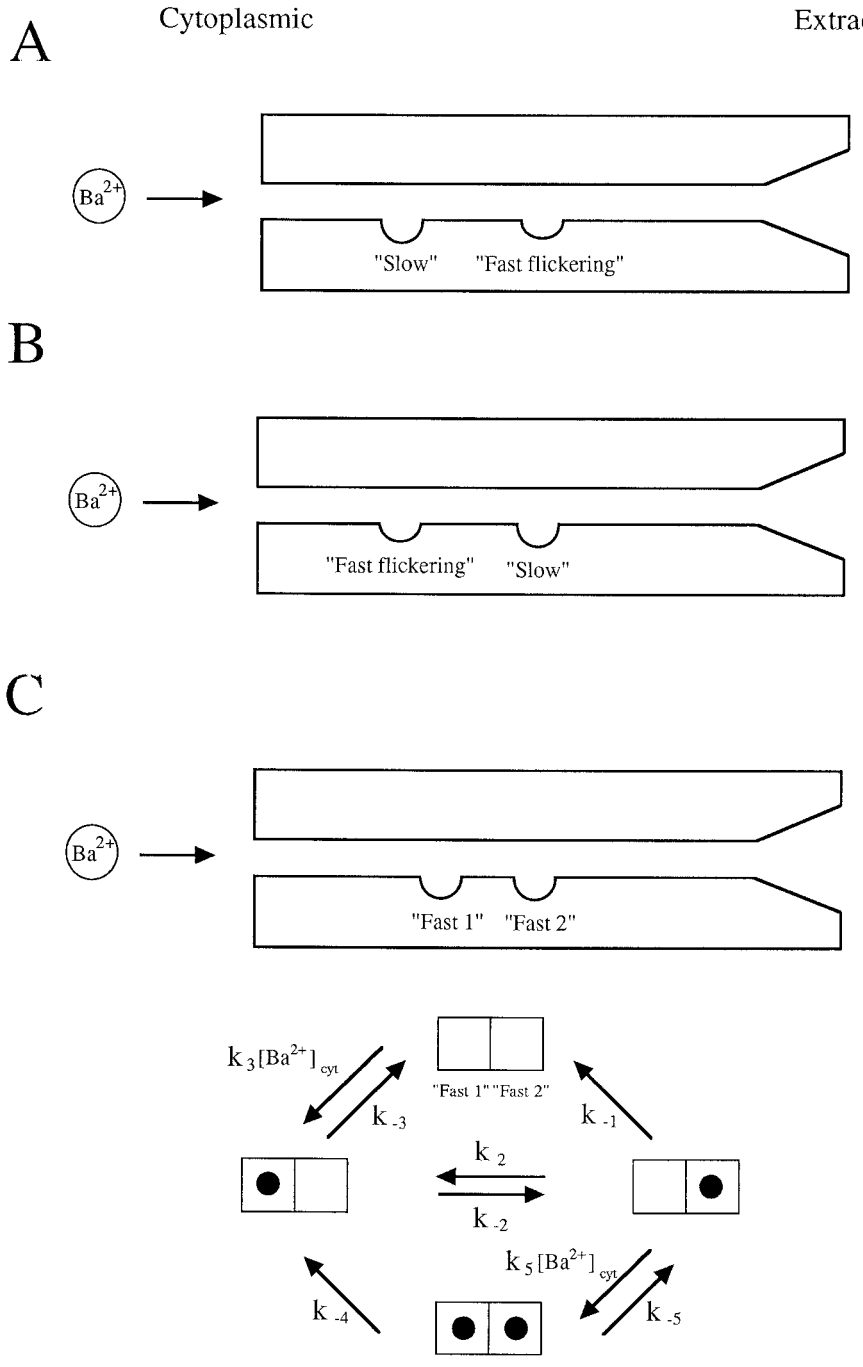

FIGURE 7 Cartoons depicting (*A*, *B*) a two-independent-site model and (*C*) a four-state cyclic equilibrium model of the human vas deferens epithelial maxi-K^+ channel. The slow site refers to the binding site responsible for the voltage-dependent "slow" block induced by internal barium. For simplicity, the site responsible for "slow" external barium block, which is located in the extracellular mouth of the channel pore, has not been included (see figure 8 of Sohma et al., 1996).

(Fig. 6 *C* and Sohma et al., 1996). In the case where Ba^{2+}, entering the channel from either the internal or external solution, dissociates to the internal side (e.g., under asymmetrical K^+ conditions, with high extracellular K^+), and assuming that $k_2 < k_{-3}$ and that $k_{-2} \ll k_{-3}$, external Ba^{2+} will first bind to the "fast 2" site and then to the "fast 1" site, and finally will dissociate to the internal side of the channel, producing "flickering block." In this case k_{f-1} is mainly dependent on k_2 in the two-binding-site scheme. On the other hand, internal Ba^{2+} will first bind to the "fast 1" site and then dissociate back to the internal side of the channel, producing the "fast flickering" block. In this case k_{ff-1} is equal to k_{-3} and should be faster than k_{f-1}, which was observed.

Our finding that the K_d for the long-lived block showed a proportional and not a square-law dependence on barium concentration would seem to be inconsistent with the double-occupancy model. However, because we could only measure over a relatively narrow concentration range, it is possible that we were unable to detect any square-law dependence. For example, the double-occupancy model has a Ba^{2+} concentration-independent step k_{-2} within the blocking sequence: $k_3 \cdot [Ba^{2+}] \rightarrow k_{-2} \rightarrow k_5 \cdot [Ba^{2+}]$. Therefore, assuming that $k_{-2} \ll k_5 \cdot [Ba^{2+}]$ and $k_2 +$

$k_{-1} < k_5 \cdot [Ba^{2+}]$, the Ba^{2+} concentration dependence of the on rate is mainly determined by the step $k_3 \cdot [Ba^{2+}]$. Under this condition, the on rate may display a proportional, and not a square-law, dependence on Ba^{2+} concentration for a small amount of block and/or over a narrow concentration range. Although double occupancy may be energetically unfavorable because of ion-ion repulsion (Newland et al., 1992), there is a possibility that a strong interaction between the channel pore and Ba^{2+} ion might make the double-occupancy state stable. Although our novel blocking scheme is just one of many, the model suggests that the "slow" block induced by internal Ba^{2+} arises from multiple barium ions binding to the channel pore.

Although our data have identified a novel type of fast channel block, there is evidence that fast block does occur in other channels. Brown et al. (1988) reported that in addition to the classical "slow" block, high concentrations of internal Ba^{2+} also reduced the single-channel conductance of a maxi-K^+ channel from *Necturus* choroid plexus, suggesting that Ba^{2+} rapidly occupied or reoccupied a site at a rate high enough to prevent the full channel current from ever being resolved. McCann and Welsh (1986) also reported that internal and external Ba^{2+} reduced the conductance of K^+ channels from tracheal smooth muscle in a voltage-dependent manner. These results are consistent with Ba^{2+} producing frequent, extremely brief blocking events that can only be detected as an apparent reduction in single-channel conductance. This suggests that the "slow" block of other maxi-K^+ channels by Ba^{2+} may also involve a mechanism similar to the one we have described here, although the kinetics may be different. Taken together, we speculate that our novel scheme for Ba^{2+} block could be applicable to Ba^{2+} block of other maxi-K^+ channels.

We thank Mr. David Stephenson for his excellent technical assistance. We thank Dr. S. Oiki for useful discussions.

Funded by grants from the Cystic Fibrosis Trust and the Medical Research Council (UK).

REFERENCES

Armstrong, C. M. 1975. Potassium pores of nerve and muscle membrane. *In* Membranes: A Series of Advances, Vol. 3. G. Eisenman, editor. Marcel Dekker, New York. 325–358.

Benham, C. D., T. B. Bolton, R. J. Lang, and T. Takewaki. 1985. The mechanism of action of Ba^{2+} and TEA on single Ca^{2+}-activated K^+-channels in arterial and intestinal smooth muscle cell membranes. *Pflugers Arch.* 403:120–127.

Brown, P. D., D. D. F. Loo, and E. M. Wright. 1988. Ca^{2+}-activated K^+ channels in the apical membrane of *Necturus* choroid plexus. *J. Membr. Biol.* 105:207–219.

Diaz, F., M. Wallner, E. Stefani, L. Toro, and R. Latorre. 1996. Interaction of internal Ba^{2+} with a cloned Ca^{2+}-dependent K^+ (*hSlo*) channel from smooth muscle. *J. Gen. Physiol.* 107:399–407.

Gray, M. A., J. R. Greenwell, and B. E. Argent. 1988. Secretin-regulated chloride channel on the apical plasma membrane of pancreatic duct cells. *J. Membr. Biol.* 105:131–142.

Gray, M. A., J. R. Greenwell, A. J. Garton, and B. E. Argent. 1990. Regulation of maxi-K^+ channels on pancreatic duct cells by cyclic AMP-dependent phosphorylation. *J. Membr. Biol.* 115:203–215.

Hamill, O. P., A. Marty, E. Neher, B. Sakmann, and F. J. Sigworth. 1981. Improved patch-clamp techniques for high-resolution current recording from cells and cell-free membrane patches. *Pflugers Arch.* 391:85–100.

Harris, A., and L. Coleman. 1989. Ductal epithelial cells cultured from human foetal epididymis and vas deferens: relevance to sterility in cystic fibrosis. *J. Cell Sci.* 92:687–690.

Hille, B., and W. Schwarz. 1978. Potassium channels as multi-ion single-file pores. *J. Gen. Physiol.* 72:409–442.

Hurst, R. S., R. Latorre, L. Toro, and E. Stefani. 1995. External barium block of *Shaker* potassium channels: evidence for two binding sites. *J. Gen. Physiol.* 106:1069–1087.

Hurst, R. S., L. Toro, and E. Stefani. 1996. Molecular determinants of external barium block in *Shaker* potassium channels. *FEBS Lett.* 388: 59–65.

Lattore, R., and C. Miller. 1983. Conduction and selectivity in potassium channels. *J. Membr. Biol.* 71:11–30.

Lopez, G. A., Y. N. Jan, and L. Y. Jan. 1994. Evidence that the S6 segment of the *Shaker* voltage-gated K^+ channel comprises part of the pore. *Nature.* 367:179–182.

McCann, J. D., and M. J. Welsh. 1986. Calcium-activated potassium channels in canine airway smooth muscle. *J. Physiol. (Lond.).* 372: 113–127.

McManus, O. B. 1991. Calcium-activated potassium channels: regulation by calcium. *J. Bioenerg. Biomembr.* 23:537–560.

Miller, C., R. Latorre, and I. Reisin. 1987. Coupling of voltage-dependent gating and Ba^{++} block in the high-conductance, Ca^{++}-activated K^+ channel. *J. Gen. Physiol.* 90:427–449.

Newland, C. F., J. P. Adelman, B. L. Tempel, and W. Almers. 1992. Repulsion between tetraethylammonium ions in cloned voltage-gated potassium channels. *Neuron.* 8:975–982.

Neyton, J., and C. Miller. 1988a. Potassium blocks barium permeation through a calcium-activated potassium channel. *J. Gen. Physiol.* 92: 549–567.

Neyton, J., and C. Miller. 1988b. Discrete Ba^{2+} blocks as a probe of ion occupancy and pore structure in the high-conductance Ca^{2+}-activated K^+ channel. *J. Gen. Physiol.* 92:569–586.

Neyton, J., and M. Pelleschi. 1991. Multi-ion occupancy alters gating in high-conductance, Ca^{2+}-activated K^+ channels. *J. Gen. Physiol.* 97: 641–665.

Perez, G., A. Lagrutta, J. P. Adelman, and L. Toro. 1994. Reconstitution of expressed K_{Ca} channels from *Xenopus* oocytes to lipid bilayers. *Biophys. J.* 66:1022–1027.

Pongs, O. 1992. Molecular biology of voltage-dependent potassium channels. *Physiol. Rev.* 72:S69–S88.

Sheppard, D. N., F. Giraldez, and F. V. Sepulveda. 1988. Kinetics of voltage and Ca^{2+} activation and Ba^{2+} blockade of a large-conductance K^+ channel from *Necturus* enterocytes. *J. Membr. Biol.* 105:65–75.

Slesinger, P. A., Y. N. Jan, and L. Y. Jan. 1993. The S4–S5 loop contributes to the ion-selective pore of potassium channels. *Neuron.* 11:739–749.

Sohma, Y., A. Harris, C. J. C. Wardle, B. E. Argent, and M. A. Gray. 1996. Two barium binding sites on a maxi-K^+ channel from human vas deferens epithelial cells. *Biophys. J.* 70:1316–1325.

Sohma, Y., A. Harris, C. J. C. Wardle, M. A. Gray, and B. E. Argent. 1994. Maxi-K^+ channels on human vas deferens epithelial cells. *J. Membr. Biol.* 141:69–82.

Vergara, C., and R. Latorre. 1983. Kinetics of Ca^{2+}-activated K^+ channels from rabbit muscle incorporated into planar bilayers. Evidence for a Ca^{2+} and Ba^{2+} blockade. *J. Gen. Physiol.* 82:543–568.

Woodhull, A. M. 1973. Ionic blockage of sodium channels in nerve. *J. Gen. Physiol.* 61:687–708.

Yellen, G. 1984. Relief of Na^+ block of Ca^{++}-activated K^+ channels by external cations. *J. Gen. Physiol.* 84:187–199.